Effect of Grain Orientation on Surface Damage of Niobium Doped Tungsten with Helium Implantation

Yutian Ma, Junbiao Liu, Han Li, Long Cheng, Ying Zhang and Kaigui Zhu

Abstract Niobium doped tungsten was irradiated by helium ion implantation, and the effect of grain orientation on surface damage induced by helium sputtering was studied by X-ray photoelectron spectroscopy, scanning electron microscopy, atomic force microscopy and electron backscattered diffraction. Many cavities or pores caused by helium sputtering were observed on the surface of the samples, and the surface damage of tungsten by helium irradiation was aggravated by 1.0×10^{18} Nb/cm^2 doping. It was found that the surface damage of different crystal orientations was distinct under same helium implantation condition. The surface damage of grains with (1 1 0) orientation was worse than that of grains with (1 1 1) and (1 0 0) orientation. The result suggested that the surface damage induced by helium sputtering was closely related to helium implantation fluence and grain orientation.

Keywords Tungsten · Helium implantation · Sputtering · Grain orientation

Introduction

Tungsten, due to its unique low sputtering and erosion rate, is a candidate plasma-facing material for controlled fusion devices like ITER [1–3]. However, it is confined by the interaction between the activated plasma and the wall, since sputtering at tungsten surface may occur when the wall is irradiated by He produced by (n, α) reactions, leading to instability and reduction of the quality of the plasma. These effects are particularly crucial in the divertor of a tokamak reactor design. Another major consequence is the long-term gradation of the mechanical properties of the wall material.

Y. Ma · J. Liu · H. Li
Institute of Electrical Engineering, Chinese Academy of Sciences, Beijing 100190, China
e-mail: guangxima888@126.com

Y. Ma · L. Cheng · Y. Zhang (✉) · K. Zhu
Department of Physics, Beihang University, Beijing 100191, China
e-mail: zhyi@buaa.edu.cn

Y. Han (ed.), *Advances in Energy and Environmental Materials*,
Springer Proceedings in Energy, https://doi.org/10.1007/978-981-13-0158-2_14

In the field of materials for fusion, many studies focusing on helium blistering behavior in tungsten have already been performed [4–6], and the research for He sputtering of tungsten has turned up in recent years [7–11]. It is well-known that He has a strong tendency to precipitate into cluster in tungsten via a variety of possible diffusion mechanisms, and the coalescence and growth of clusters are able to produce swelling and blistering, which results in the surface damage. The He-induced surface damage caused by helium blistering and helium sputtering, which caused significant morphology changes in the surface of tungsten. Depending on the irradiation condition, different changes in the microstructure of tungsten occur, such as fuzz growth at elevated exposure temperature [10]. In addition, the grain orientation affected the He-induced surface damage has been reported in some literatures [12–15]. This is interesting as it may provide an approach to understand the helium behavior in tungsten. Recently, Hou et al. simulated the damage induced by helium implantation for crystalline tungsten with (1 0 0), (1 1 0) and (1 1 1) by the Binary Collision Approximation, and found that the He backscattering yields follow the same scaling: 8% on (1 1 0), 4% on (1 0 0), 3% on (1 1 1) [16]. Sefta et al. simulated (1 0 0) and (1 1 0) surfaces damage induced by helium ion exposure in the range of 300 eV–1 keV by Molecular Dynamics, and revealed that sputtering is higher for (1 1 0) surfaces relative to (1 0 0) surfaces [17]. Becquart et al. simulated formation energies for different configurations of the self-interstitial atoms in tungsten (1 0 0), (1 1 0) and (1 1 1) surfaces, and found that the (1 1 1) dumbbell to be the most stable in tungsten [18]. Based on the above theoretical research, the related experimental studies are necessary to investigate the effect of grain orientation on surface damage induced by helium ions.

Doping elements in tungsten could improve its property. Tungsten and niobium (Nb) could form solute solid and the addition of niobium in tungsten could improve mechanical property such as ductility and strength. In our previous work, two kinds of W materials, i.e. pure tungsten and niobium doped tungsten, were studied with helium ion implantation [19]. It was found that niobium doped tungsten had improved helium sputtering resistance compared to pure tungsten. Grain orientation effects in sputtering have been reported by Manova et al. [20, 21] and Michaluk, et al. [22]. In this work, niobium-doped tungsten samples were implanted with helium as previous [19], and the surface damage as a function of grain orientation was investigated. We found that grains with (1 1 0) orientation were most severely damaged by helium sputtering, and grains having (1 1 1) orientation were damaged the least. The relative height of grains as a function of surface orientation following He implantation was used to show the relation between surface damage and orientation.

Experiment Description

Pure tungsten plate was prepared by powder-metallurgy and hot-rolled reduction, with a purity of 99.99 wt%. Samples used in the experiments were cut into 10 mm × 10 mm × 3 mm-thick from the plates and polished on one side. Each one was cleaned in an acetone ultrasonic bath before testing. Niobium was implanted into tungsten with an incident energy of 45 keV and fluence of 1.0×10^{18} Nb/cm^2 using an ion implanter equipped with Metal Vapor Vacuum Arc (MEVVA). The background pressure was lower than 1.0×10^{-5} Pa, and the working pressure of helium around the sample holder was 1 Pa. The incident energy of helium was about 40 keV with a flux of 1.5–2.0 $\times$ 10^{13} ion/cm^2/s and the incident fluence were varied via choosing different irradiation durations from 3.0×10^{16} to 3.6×10^{17} He/cm^2. During each implantation, the sample surface temperature was kept below 400 K by water cooling.

The surface compositions were analyzed by X-ray photoelectron spectroscopy (XPS) since the samples were implanted with niobium. The XPS spectra of Nb was measured at a pass energy of 20 eV and an energy step of 0.2 eV. The original surface was sputtered using 1 keV argon (Ar) ions for 1, 2, 4, 6, 8, and 10 min. The Ar ion etching rate is estimated to be 0.08 nm/s.

The surface damage of irradiated samples was observed with scanning electron microscope (SEM) and atomic force microscopy (AFM). Electron backscattered diffraction (EBSD) was employed to examine grain orientation.

Results and Discussion

Surface Composition. Figure 1 shows the XPS spectra of Nb 3d. The two peaks at 203 and 206 eV are due to the metallic state of Nb, i.e. Nb 3d5/2 and Nb 3d3/2, respectively. Moreover, two peaks near 210 and 207.5 eV in the case of no etching were observed, which correspond to the Nb 3d3/2 and Nb 3d5/2 bands in Nb_2O_5, respectively. However, Nb–W intermetallic compounds were not observed in the Nb 3d spectrum as shown in Fig. 1a, which indicates no formation of Nb–W intermetallic compounds during Nb implantation. Though the peak of Nb concentration reached 8.32 at% after 1.0 × 1018 Nb/cm^2 as shown in Fig. 1b, no

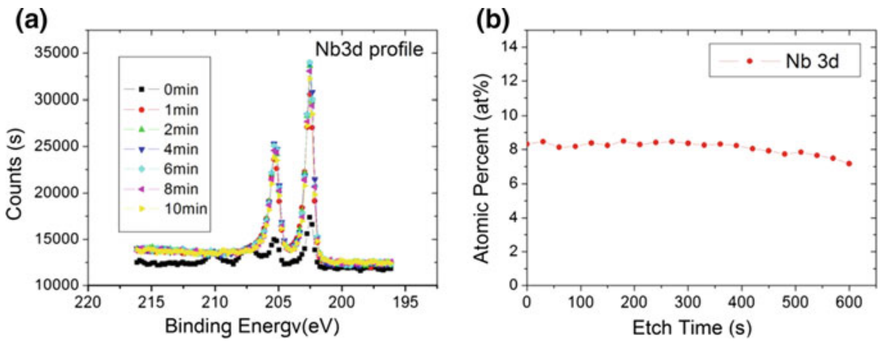

Fig. 1 Nb 3d spectra (**a**) and atomic percents of Nb as a function of sputtering time (**b**) in tungsten samples implanted with 1.0×10^{18} Nb/cm^2

Nb–W intermetallic compound was formed due to the low sample temperature. These results suggest that Nb is mainly a metal dopant in solution in tungsten.

Surface Damage. The surface morphology changes of Nb doped tungsten as a function of He implantation fluence is shown in Fig. 2. Compared with surface morphology of un-irradiated sample as shown in Fig. 2a, a lot of nano-size cavities were observed on the surface of sample irradiated with 3×10^{16} He/cm^2 as shown in Fig. 2b, which due to helium sputtering since the irradiation energy is much higher than the sputtering threshold of tungsten (50 eV). However, under higher irradiation fluence, the amount and density of cavities decreased and many pores appeared on surface of sample as shown in Fig. 2c, and the diameters of pores were in the range of 50–100 nm. With increasing He fluence, the average diameter of the surface pores increased and the cavities disappeared at the fluence of 1.2×10^{17} He/cm^2 as shown in Fig. 2d. Besides, these pores had a coalescence process and tended to form bigger pores with higher He fluence as shown in Fig. 2e [23]. These pores varied in shape during their coalescence process, from circle pore to long groove, which indicates that the coalescence happened under certain orientations at the fluence of 3.6×10^{17} He/cm^2, the evolution of coalescence resulted in the formation of "coral" type surface structures as observed in Fig. 2f. Similar surface morphology was reported previously [24]. In addition, the surface was strongly corrugated with protrusions arranged along parallel lines as shown in Fig. 2e and more obvious with higher He fluence as shown in Fig. 2f, which is similar to surface morphology reported by Manova [20]. From the result, the surface morphology changed obviously, and the change is closely related with the helium irradiation fluence.

The irradiated surfaces were also observed at a tilting angle of 70° and a special surface morphology by helium sputtering was observed at low magnification. At the

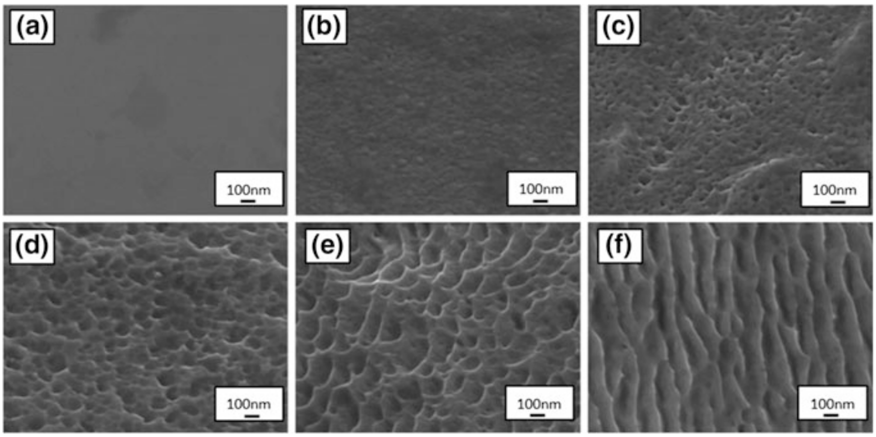

Fig. 2 Surface topographies of 1×10^{18} ions/cm^2 Nb doped tungsten samples irradiated by 40 keV He with various fluences: **a** 0, **b** 3.0×10^{16} He/cm^2, **c** 6.0×10^{16} He/cm^2, **d** 1.2×10^{17} He/cm^2, **e** 2.4×10^{17} He/cm^2, and **f** 3.6×10^{17} He/cm^2

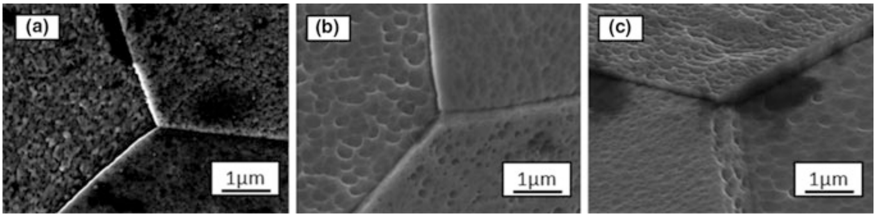

Fig. 3 Surface topographies of 1.0×10^{18} ions/cm^2 Nb doped tungsten samples irradiated by 40 keV He with various fluences: **a** 1.2×10^{17} He/cm^2, **b** 2.4×10^{17} He/cm^2, and **c** 3.6×10^{17} He/cm^2

fluence of 1.2×10^{17}, 2.4×10^{17} and 3.6×10^{17} He/cm^2, three adjacent grains demonstrate different heights as shown in Fig. 3. The grain height difference induced by He sputtering was prominent with increasing He implantation fluence as shown in Fig. 3a–c. Moreover, the difference in the surface morphology was observed, which changes thoroughly from grain to grain with very sharp grain boundaries, and the similar phenomenon has been reported in the literature [12]. The difference of surface morphology is not correlated with the direction of the ion beam as discussed in the literature [12], since an identical with implantation angle was used in this work. Thus, the surface damage is considered to be related to grain crystal orientation. However, this phenomenon was not observed in pure tungsten, 1.0×10^{16} Nb/cm^2 doped tungsten and 1.0×10^{17} Nb/cm^2 doped tungsten under same helium implantation condition in our previous work. According to the results of first-principle computations by Wu et al. [25], the phenomenon may attribute to the following reason: Nb as an impurity implanted into tungsten decreased the charge density and increased the binding energy, resulted in the aggregation of He atoms around the impurities, which enhanced the He damage in tungsten.

EBSD Analysis. The EBSD measurement was done in the area of 18×15 μm^2 with a scanning step of 0.5 μm/min on a hexagonal grid for samples shown in Fig. 3. The EBSD map of sample (same sample as in Fig. 3b) irradiated by 40 keV He ion beam with 2.4×10^{17} He/cm^2 was shown in Fig. 4. The individual grains were marked as a, b, c in both the SEM image and EBSD map. According to EBSD measurement, the three orientations of (1 0 0), (1 1 0) and (1 1 1) were present on the surface, and the grain orientation of a, b, c corresponds to (1 1 1), (1 0 0), and (1 1 0), respectively. It can be clearly seen that the height of grain with (1 1 0) orientation was lower than that of other two grains, and the height of grain with (1 1 1) orientation was the highest. In other words, the grain with (1 1 0) orientation was damaged worse than the other two grains, and the damage of grain with (1 1 1) orientation was the slightest. The EBSD result of the two other samples (same sample as Fig. 3a, c respectively) irradiated by He ion beam with 1.2×10^{17} and 3.6×10^{17} He/cm^2 as shown in Fig. 5a, b, respectively. Similar phenomenon was observed, which proved that there is a strong correlation between the surface damage and grain orientation. The surface height difference indicates that the

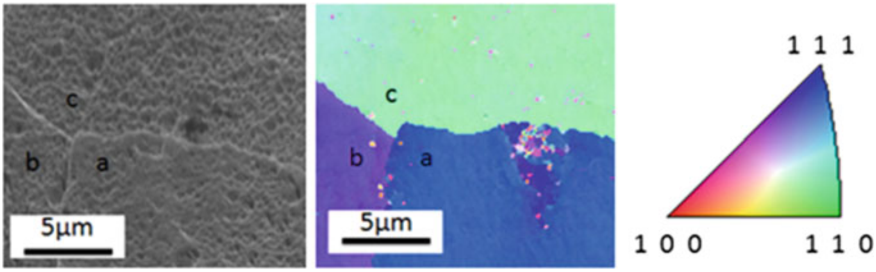

Fig. 4 EBSD map of sample irradiated by 40 keV He with 2.4×10^{17} He/cm^2

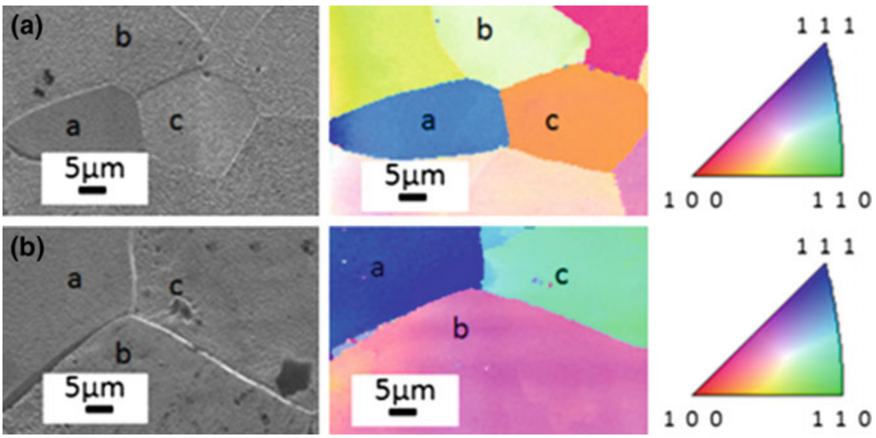

Fig. 5 EBSD map of sample irradiated by 40 keV He with **a** 1.2×10^{17} He/cm^2, **b** 3.6×10^{17} He/cm^2

helium sputtering yield of different crystalline planes $Y_{(UVW)}$ for tungsten, which can be calculated from the FIB experiment by the following formula [26]:

$$Y_{(UVW)} = \frac{N_{target}}{N_{ion}} = \frac{\frac{N_A \cdot V \cdot \rho}{m_{t\arg et}}}{\frac{i \cdot t}{e}} = \frac{e \cdot N_A \cdot A \cdot h_{(UVW)} \cdot \rho}{m_{t\arg et} \cdot i \cdot t} \quad (1)$$

where e is the elementary charge, N_A is the Avogadro constant, A is the sputtering area, $h_{(UVW)}$ is the erosion depth of a tungsten crystalline plane, ρ is the tungsten target density, mtarget is the tungsten atom weight, i is the ion beam current, and t is the sputtering time.

AFM Measurement. The step heights between the surfaces of different grain orientations discussed above were further measured with AFM scanning. Figure 6 shows the AFM images of the scanning results with the values of height difference between (1 0 0), (1 1 0), (1 1 1) orientations. The grain orientation of (1 1 1), (1 0 0), and (1 1 0) was marked as a, b and c, respectively. The height difference between (1 1 1) and (1 0 0) is marked as h_{ab}, the height difference between (1 1 1) and (1 1 0) was marked as h_{ac}, and the height difference between (1 0 0) and (1 1 0) was marked as h_{bc}. For Nb doped tungsten (same as Fig. 3a) irradiated with

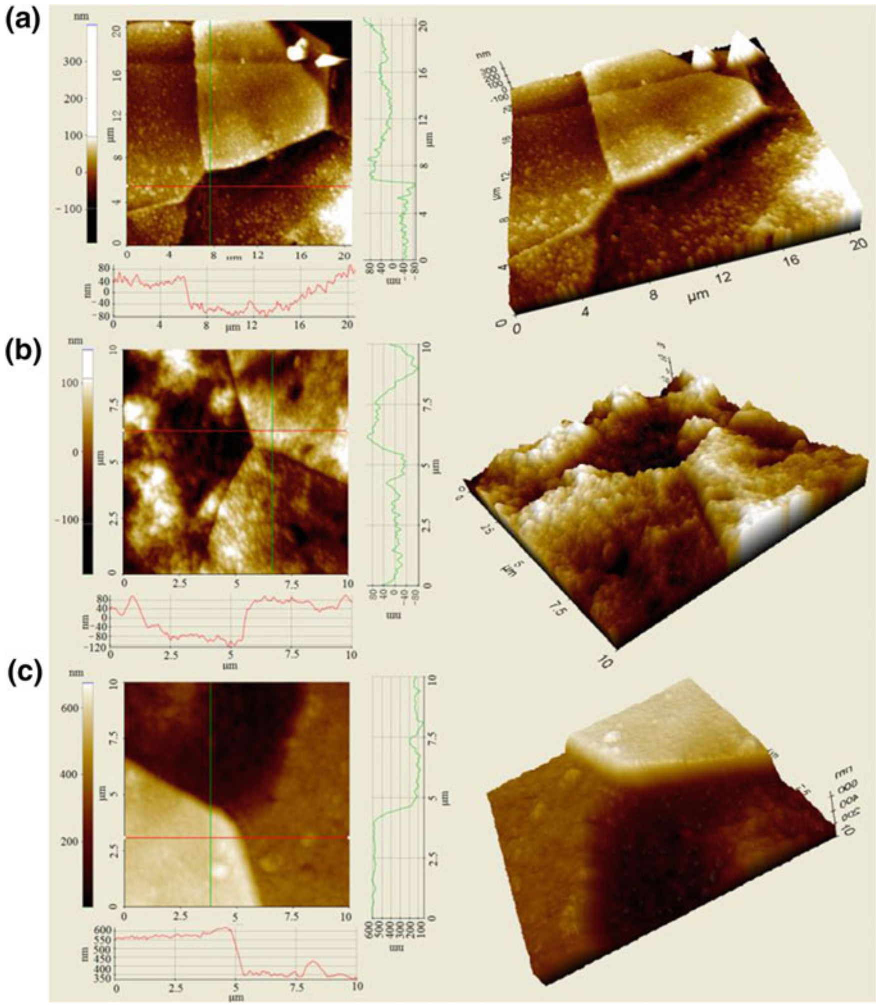

Fig. 6 2D and 3D AFM images of 1.0 × 10^{18} ions/cm^2 Nb doped tungsten samples irradiated by 40 keV He with various fluences: **a** 1.2 × 10^{17} He/cm^2, **b** 2.4 × 10^{17} He/cm^2, and **c** 3.6 × 10^{17} He/cm^2

1.2×10^{17} He/cm^2 as shown in Fig. 6a, h_{ab}, h_{bc} and h_{ac} was 40, 80 and 120 nm, respectively. Corresponding to the samples (same as Fig. 3b, c, respectively) as shown in Fig. 6b, h_{ab}, h_{bc} and h_{ac} is 80, 80 and 160 nm for 2.4×10^{17} He/cm^2, and in Fig. 6c, h_{ab}, h_{bc} and h_{ac} was 250, 250 and 500 nm for 3.6×10^{17} He/cm^2. This indicates that the helium sputtering rate of different crystal surface was different and the sputtering rate increases with the helium fluence increasing. In addition, the measured height of individual grains by AFM could be converted by Eq. (1) to obtain the sputtering yield for tungsten. The sputtering yield of (1 1 0) plane was the highest, followed by that of (1 0 0) plane, while that of (1 1 1) plane was the lowest. The results are agreed with the sputtering yield of molybdenum by Huang [26].

First-Principles Computation. The relationship between surface damage and grain orientation was studied with the first-principles computation. Density functional theory (DFT) calculations were performed with the Vienna Ab Initio Simulation Package (VASP) [27, 28]. The W-6 s 5d were treated as valence electrons, while the ionic cores were represented by the projector augmented wave (PAW) potentials [29]. The exchange and correlation interaction among electrons were described at the level of the generalized gradient approximation (GGA) using the Perdew–Burke–Ernzerhof (PBE) formula [30]. The kinetic energy cutoff for the plane-wave basis set was set to 400 eV, which kept the total energy errors below 1 meV. The first-order Methfessel–Paxton method [31] was used for the Fermi surface smearing, with a width of 0.2 eV. The convergence criteria for the electronic self-consistent iteration and the ionic relaxation loop were set to 10–5 eV and 0.01 eV/Å, respectively. As for the W bulk, the k-point sampling was chosen with $8 \times 8 \times 8$ net-grid which keeps the total energy errors below 10 meV. The calculated lattice constant 3.175 Å were agreed well with experimental value 3.165 Å. Three typical of low Miller index surfaces of W (1 0 0) (1 1 0) (1 1 1) were investigated here. Three surface models of W (1 0 0) (1 1 0) and (1 1 1) surface are shown in Fig. 7. The surface slabed models with a dimension of 3×3 for (100), 3×2 for (1 1 0) and 3×3 for (1 1 1) surface. The atom layer was chosen with 9

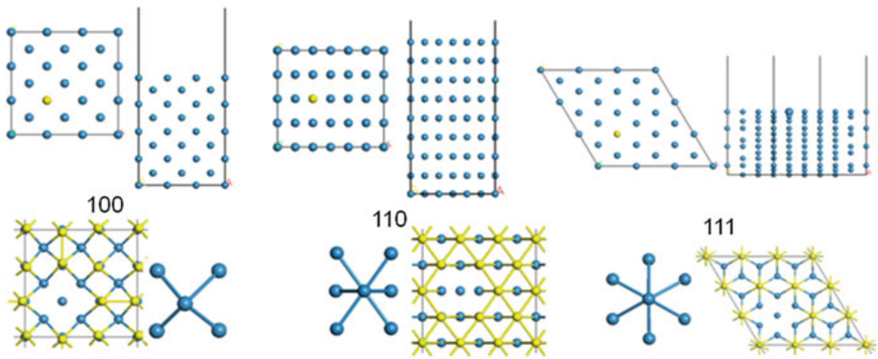

Fig. 7 Three surface models of W (1 0 0) (1 1 0) and (1 1 1) surface. The blue balls represent tungsten atoms, and the yellow balls in the surface will be taken away in the later

Table 1 Atomic surface density, surface energy and escape energy of different crystal

Crystal	Surface atomic density (atoms/Å2)	Surface energy (eV/Å2)	Escape energy (eV)
(1 0 0)	0.09919	0.247	10.470484
(1 1 0)	0.14028	0.201	12.845554
(1 1 1)	0.05726	0.217	11.469154

layers for (1 0 0) and (1 1 0), 12 layers for (1 1 1). The k-point sampling was chosen as $3 \times 3 \times 1$ for (1 0 0) and (1 1 0), $2 \times 2 \times 1$ for the (1 1 1) surface. Only the bottom atom layer was fixed to mimic the semi-infinite crystal for all calculations.

According to the first-principles computations, the atomic distance, surface atomic density, surface energy and escaping energy are listed in Table 1. The follow equation was used to calculate the escapeenergy: Eesc = En_{-1} + Ew − En, in which, Ew is the energy of one tungsten atom in bulk, En and En−1 are the energy of slab and the energy of slab with one atom taken away from the surface layer, respectively. The escaping energy is the energy needed to take away one surface atom which represents the stability of the surface. From Table 1, it is found that the escaping energy varied with the surface energy, that is, the lower the surface energy was, the higher the escaping energy. With physical intuitively, under the same irradiation condition, the surface damage would be more moderate with higher escaping energy, that is to say, the (1 1 0) surface would be have the slightest surface damage due to its highest escaping energy. While the (1 1 0) surface has the highest escaping energy and the smallest surface energy, but the (1 1 0) surface has the most serious surface damage under the He ions irradiation as shown in our experiments.

The surface atomic densities are calculated as following 0.05726/$Å^2$, 0.09919/$Å^2$ and 0.14028/$Å^2$ for (1 1 1), (1 0 0) and (1 1 0), respectively. The atomic surface density of (1 1 0) surface is the largest and it is almost triple time of (1 1 1) surface. The result of the atomic surface density calculation demonstrate different planar packing fraction (f) at different orientations, that is f (1 1 0) > f (1 0 0) > f (1 1 1). This agrees with the result from molybdenum, another bcc metal [26]. Difference of damage level at different orientations can be explained by the variation of the planar packing fraction. According to the literature [32, 33], the surface sputtering happens when atoms at sub-surface layer receive enough momentum via collision cascade events. At the orientation of the highest planar packing fraction the penetration of implantation particles suffers the greatest retarding based on the crystalline transparency model [34, 35]. The momentum transfer happens at the shallowest depth, compared with the other two orientations, resulting to the most severe damage on the surface [36]. With this notion, we can explain why (1 1 0) surface has the most serious damage, (1 0 0) takes second place and (1 1 1) has the slightest surface damage.

Conclusions

Helium ion implantation has been carried out on niobium doped tungsten. The surface damage induced by helium implantation was characterized and discussed. The Nb was implanted into tungsten and existed in atomic states on tungsten substrate. Many cavities or pores caused by helium sputtering were observed on the surface of sample, and the surface damage of tungsten by helium irradiation was aggravated by 1.0×10^{18} Nb/cm^2 doping. It was found that the surface damage is related with grain orientation. The damage of grain with (1 1 0) orientation is the most, while that of grain with (1 1 1) orientation is the slightest. The surface damage difference is owing to the atomic surface density in grain with different crystal orientation.

Acknowledgements This research is supported by the National Magnetic Confinement Fusion Programs with Grant No. 2013GB109003, and the National Natural Science Foundation of China with Grant No. 51171006, and Scientific Research equipment development project of Chinese Academy of Sciences (with Grant No. YZ201410).

References

1. J. Roth, E. Tsitrone, A. Loarte, et al., Recent analysis of key plasma wall interactions issues for ITER. J. Nucl. Mater. **390–391**, 1–9 (2009)
2. H. Bolt, V. Barabash, G. Federici, et al., Plasma facing and high heat flux materials—needs for ITER and beyond. J. Nucl. Mater. **307–311**, 43–52 (2002)
3. H. Bolt, V. Barabash, W. Krauss, et al., Materials for the plasma-facing components of fusion reactors. J. Nucl. Mater. **329–333**, 66–73 (2004)
4. K. Tokunaga, R.P. Doerner, R. Seraydarian, et al., Surface morphology and helium retention on tungsten exposed to low energy and high flux helium plasma. J. Nucl. Mater. **313–316**, 92–96 (2003)
5. D. Nishijima, M.Y. Ye, N. Ohno, et al., Incident ion energy dependence of bubble formation on tungsten surface with low energy and high flux helium plasma irradiation. J. Nucl. Mater. **313–316**, 1029–1033 (2004)
6. S.B. Gilliam, S.M. Gidcumb, N.R. Parikh, et al., Retention and surface blistering of helium irradiated tungsten as a first wall material. J. Nucl. Mater. **347**, 289–297 (2005)
7. M. Tomita, K. Masumori, Fluence- and temperature-dependence of sputtering yield by 25 keV He-ion bombardment on tungsten and niobium. Nucl. Instr. Methods B. **39**, 95–98 (1989)
8. M.J. Baldwin, R.P. Doerner, Formation of helium induced nanostructure 'fuzz' on various tungsten grades. J. Nucl. Mater. **404**, 165–173 (2010)
9. A. Lasa, K.O.E. Henriksson, K. Nordlund, MD simulations of onset of tungsten fuzz formation under helium irradiation. Nucl. Instr. Methods B. **303**, 156–161, (2013)
10. D. Nishijima, M.J. Baldwin, R.P. Doerner, et al., Sputtering properties of tungsten 'fuzzy' surfaces. J. Nucl. Mater. **415**, 96–99 (2011)
11. K. Katayama, K. Imaoka, T. Okamura, et al., Helium and hydrogen trapping in tungsten deposition layers formed by helium plasma sputtering. Fusion Eng. Des. **82**, 1645–1650 (2007)
12. B.M.U. Scherzer, in *Development of Surface Topography Due to Gas Ion Implantation*, ed. by R. Behrisch. Sputtering by Particle Bombardment, (Springer, Berlin, 1981) pp. 271–355

13. C. Li, H. Greuner, Y. Yuan, et al., Effects of temperature on surface modification of W exposed to He particles. J. Nucl. Mater. **455**, 201–206 (2014)
14. N. Ohno, Y. Hirahata, M. Yamagiwa, et al., Influence of crystal orientation on damages of tungsten exposed to helium plasma. J. Nucl. Mater. **438**, 879–882 (2013)
15. C.M. Parish, H. Hijazi, H.M. Meyer, et al., Effect of tungsten crystallographic orientation on He-ion-induced surface morphology changes. Acta Mater. **62**, 173–181 (2014)
16. M. Hou, C.J. Ortiz, C.S. Becquart, et al., Microstructure evolution of irradiated tungsten: crystal effects in He and H implantation as modelled in the binary collision approximation. J. Nucl. Mater. **403**, 89–100 (2010)
17. F. Sefta, N. Juslin, K. D. Hammond, et al., Molecular dynamics simulations on the effect of sub-surface helium bubbles on the sputtering yield of tungsten. J. Nucl Mater. **438**, 493–496 (2013)
18. C.S. Becquart, C. Domain, Ab initio calculations about intrinsic point defects and He in W. Nucl. Instr. Methods B. **255**, 23–26 (2007)
19. Y.T. Ma, Y. Zhang, G.H. Lu, et al., Effect of helium implantation on mechanical properties of niobium doped tungsten, Sci. Chin. Phys. Mech. Astron. **56**(7), 1396–1400 (2013)
20. D. Manova, M. Schreck, S. Mändl, et al., Orientation dependent sputter yield of aluminium. Surf. Coat. Technol. **151–152**, 72–75 (2002)
21. H.K. Zhang, D.M. Liu, H.B. Li et al., Study on the microstructure of high purity aluminum sputtering targets by EBSD method. J. Chin. Electr. Microsc. Soc. **27**(6), 491–494 (2008)
22. C.A. Michaluk, Correlating discrete orientation and grain size to the sputter deposition properties of tantalum. J. Electron Mater. **31**(1), 1–9 (2002)
23. S. Sharafat, A. Takahashi, K. Nagasawa et al., A description of stress driven bubble growth of helium implanted tungsten. J. Nucl. Mater. **389**, 203–212 (2009)
24. Q. Xu, N. Yoshida, T. Yoshiie, Accumulation of helium in tungsten irradiated by helium and neutrons. J. Nucl. Mater. **367–370**, 806–811 (2007)
25. X-B. Wu, X-S. Kong, Y-W. You, et al., First principles study of helium trapping by solute elements in tungsten. J. Nucl. Mater. **455**, 151–156 (2014)
26. H.S. Huang, C.H. Chiu, I.T. Hong, et al., Determining the sputter yields of molybdenum in low-index crystal planes via electron backscattered diffraction, focused ion beam and atomic force microscope. Mater. Charact. **83**, 68–73 (2013)
27. G. Kresse, J. Hafner, Ab Initio Molecular Dynamics for Liquid Metals. Phys Rev B. **47**, 558–561 (1993)
28. G. Kresse, J. Furthmüller, Efficiency of Ab-Initio total energy calculations for metals and semiconductors using a plane-wave basis set. Comp. Mater. Sci. **6**, 15–50 (1996)
29. G. Kresse, D. Joubert, From ultrasoft pseudopotentials to the projector augmented-wave method. Phys. Rev. B. **59**, 1758–1775 (1999)
30. J.P. Perdew, K. Burke, M. Ernzerhof, Generalized gradient approximation made simple. Phys. Rev. Lett. **77**, 3865–3868 (1996)
31. M. Methfessel, A.T. Paxton, High-precision sampling for Brillouin-zone integration in metals. Phys. Rev. B. **40**, 3616 (1989)
32. C. Michaluk, *Metallurgical Factors Affecting the Performance of Tantalum Sputtering Targets*, ed. by C. Culbertson. Proceedings of 41th International Symposium on Tantalum and Niobium. Brussels, Belgium: Tantalum–Niobium International Study Center, 2000, p. 75
33. R.S. Averback, T.D. Rubia, Displacement damage in irradiated metals and semiconductors. Solid State Phys. **51**, 281–402, (1997)
34. J.M. Fluit, P.K. Rol, J. Kistemaker, Angular-dependent sputtering of copper single crystals. J. Appl. Phys. **34**, 690–691 (1963)
35. A.L. Southern, W.R. Willis, M.T. Robinson, Sputtering experiments with 1- to 5-keV Ar + ions, J. Appl. Phys. **34**, 153–163 (1963)
36. G.D. Magnuson, C.E. Carlston, Electron ejection from metals due to 1- to 10-keV noble gas ion bombardment. I. polycrystalline materials. J. Appl. Phys. **34**, 3267–3273 (1963)